iScience

CellPress
OPEN ACCESS

Article

Endothelial SIRT-1 has a critical role in the maintenance of capillarization in brown adipose tissue

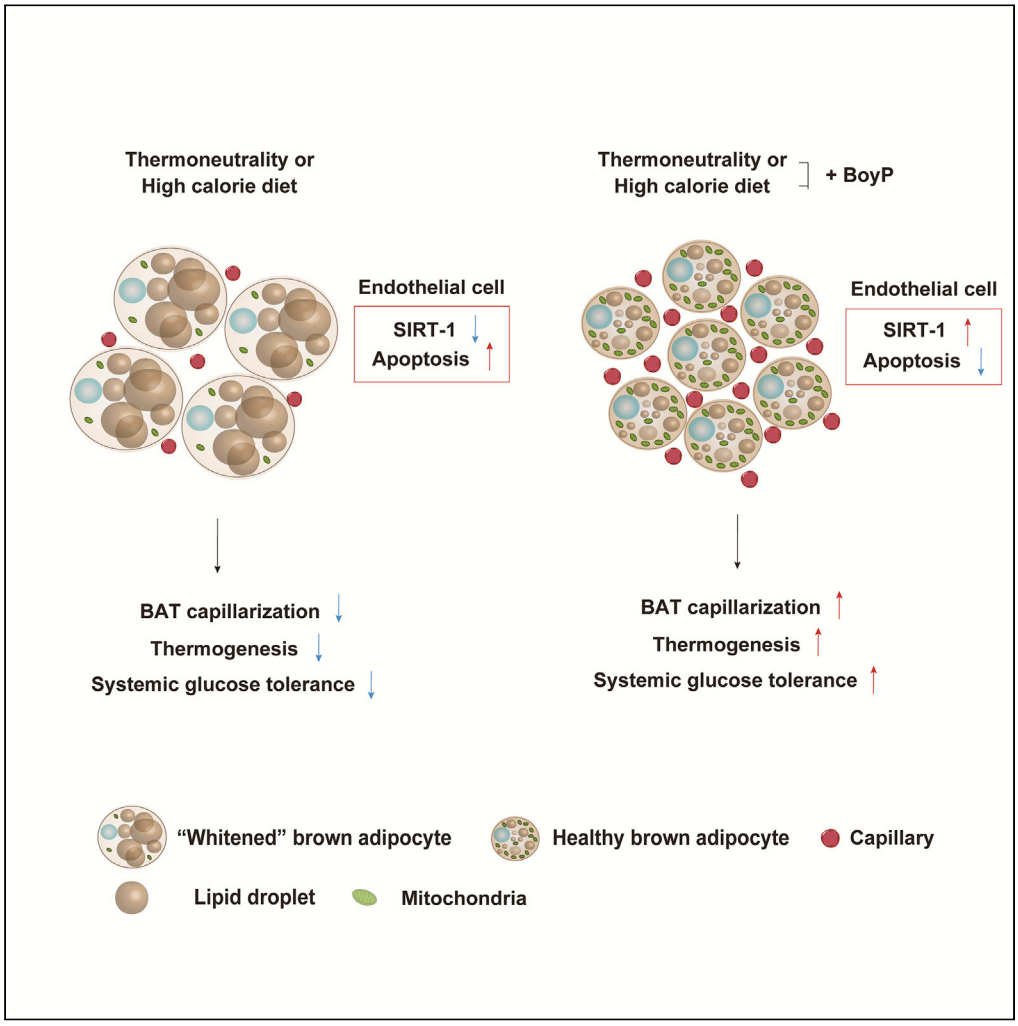

Ryo Furuuchi, Ippei Shimizu, Yohko Yoshida, ..., Yoshiaki Kubota, Kenneth Walsh, Tohru Minamino

ippeishimizu@yahoo.co.jp (I.S.)
t.minamino@juntendo.ac.jp (T.M.)

Highlights

Dietary obesity and thermoneutrality reduce SIRT-1 expression in BAT ECs

Boysenberry polyphenols increase EC SIRT-1 expression

EC SIRT-1 has a critical role in maintaining capillarization in BAT

Furuuchi et al., iScience 25, 105424
November 18, 2022
https://doi.org/10.1016/j.isci.2022.105424

iScience

CellPress
OPEN ACCESS

Article

Endothelial SIRT-1 has a critical role in the maintenance of capillarization in brown adipose tissue

Ryo Furuuchi,[1,2,3,7] Ippei Shimizu,[1,7,*] Yohko Yoshida,[1,3] Goro Katsuumi,[1] Masayoshi Suda,[1] Yoshiaki Kubota,[4] Kenneth Walsh,[5] and Tohru Minamino[1,6,8,*]

SUMMARY

Brown adipose tissue (BAT) has critical roles in thermogenesis and systemic metabolism. Capillary rarefaction was reported to develop in BAT with dietary obesity, and previous studies showed that suppression of vascular endothelial growth factor A (VEGF-A) reduced capillary density in BAT, promoting the functional decline of this organ. Capillarization is regulated through the balance between angiogenesis and vasculogenesis on the one hand and apoptosis of endothelial cells (ECs) on the other; however, the role of EC apoptosis in BAT remained to be explored. In studies testing the role of boysenberry polyphenols (BoyP) in BAT, we found that BoyP decreased EC apoptosis, enhanced capillarization in BAT, and ameliorated dietary BAT dysfunction, which was associated with the upregulation of nicotinamide adenine dinucleotide-dependent protein deacetylase sirtuin 1 (SIRT-1) in ECs. Our studies suggest that EC SIRT-1 would be one of the potential targets of BoyP that contributes to BAT capillarization and function.

INTRODUCTION

In many societies, the prevalence of obesity remains high, and the associated comorbidities, including diabetes, heart failure, and ischemic cardiovascular diseases, continue to be important health care issues (Despres et al., 2021). Skeletal muscle, liver, and adipose tissues have critical roles in maintaining systemic metabolic health (Scheja and Heeren, 2019), so enhancing the function of these tissues has the potential to become an anti-obesity treatment. Nutrients and oxygen are delivered through capillaries, and this platform is critical for maintaining the function of metabolically active organs (Stucker et al., 2021). With aging or age-related disorders, capillary rarefaction develops in systemic organs, and studies indicate that this process enhances the functional decline of these tissues and promotes pathogenesis in cardiovascular-metabolic disorders (Grunewald et al., 2021; Shimizu et al., 2014).

Brown adipose tissue (BAT) was initially characterized as a thermogenic organ, and nowadays it is well known to have critical roles in regulating systemic metabolism (Bartelt et al., 2011; Rosen and Spiegelman, 2014; Stanford et al., 2013). It was once thought to be present only in small rodents and human infants, but human adults are now also known to have functional BAT (Lichtenbelt et al., 2009). BAT activation increases energy expenditure (Lynes et al., 2017), reduces body weight (Stanford et al., 2013), and is inversely correlated with body mass index (BMI) and aging (Becher et al., 2021; Lichtenbelt et al., 2009). BAT is a mitochondria-rich organ and equipped with a dense capillary network to meet its high demand for oxygen nutrients (Shimizu et al., 2014). Dietary obesity and aging are associated with both diminished capillary density and functional decline in this organ (Shimizu et al., 2014). A genetic model with capillary rarefaction in adipose tissues induced a whitened phenotype in BAT and promoted a systemic metabolic disorder and reduced thermogenesis (Shimizu et al., 2014). Enhancing capillarization in BAT has the potential to maintain homeostasis in this tissue and systemic metabolic health; however, the mechanisms leading to increased capillarization remain to be explored.

Some food ingredients were reported to increase BAT function (Kurylowicz and Puzianowska-Kuznicka, 2020), including resveratrol, a polyphenol found in grapes (Milton-Laskibar et al., 2018; Wang et al., 2017). Resveratrol is also known as an activator of nicotinamide adenine dinucleotide-dependent protein deacetylase sirtuin 1 (SIRT-1) (Shakibaei et al., 2011), and in cardiac tissues, endothelial cell (EC) SIRT-1

[1]Department of Cardiovascular Biology and Medicine, Juntendo University Graduate School of Medicine, 2-1-1 Hongo, Bunkyo-ku, Tokyo 113-8431, Japan

[2]Bourbon Corporation, Niigata 945-8611, Japan

[3]Department of Advanced Senotherapeutics, Juntendo University Graduate School of Medicine, Tokyo 113-8431, Japan

[4]Department of Anatomy, Keio University School of Medicine, Tokyo 160-8582, Japan

[5]Division of Cardiovascular Medicine, Robert M. Berne Cardiovascular Research Center, University of Virginia School of Medicine, Charlottesville, VA 22908, USA

[6]Japan Agency for Medical Research and Development-Core Research for Evolutionary Medical Science and Technology (AMED-CREST), Japan Agency for Medical Research and Development, Tokyo 100-0004, Japan

[7]These authors contributed equally

[8]Lead contact

*Correspondence: ippeishimizu@yahoo.co.jp (I.S.), t.minamino@juntendo.ac.jp (T.M.)

https://doi.org/10.1016/j.isci.2022.105424

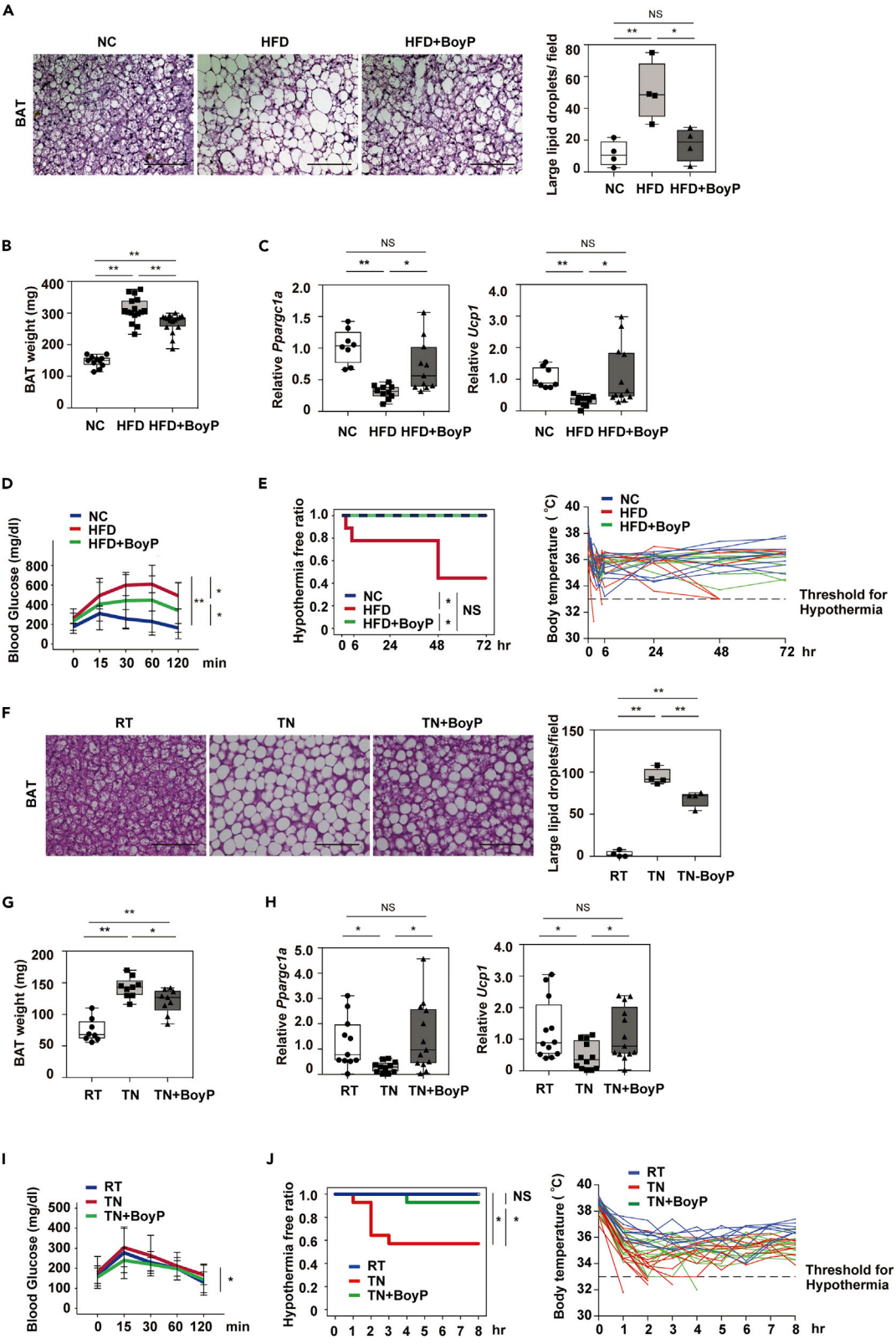
A
NC
HFD
HFD+BoyP
BAT
Large lipid droplets/ field
NS
**
*
NC HFD HFD+BoyP
B
BAT weight (mg)
NC HFD HFD+BoyP
C
Relative Ppargc1a
Relative Ucp1
NC HFD HFD+BoyP
D
Blood Glucose (mg/dl)
NC
HFD
HFD+BoyP
0 15 30 60 120 min
E
Hypothermia free ratio
NC
HFD
HFD+BoyP
NS
0 6 24 48 72 hr
Body temperature (°C)
Threshold for Hypothermia
F
RT
TN
TN+BoyP
BAT
Large lipid droplets/field
RT TN TN-BoyP
G
BAT weight (mg)
RT TN TN+BoyP
H
Relative Ppargc1a
Relative Ucp1
RT TN TN+BoyP
I
Blood Glucose (mg/dl)
RT
TN
TN+BoyP
0 15 30 60 120 min
J
Hypothermia free ratio
RT
TN
TN+BoyP
NS
0 1 2 3 4 5 6 7 8 hr
Body temperature (°C)
Threshold for Hypothermia

Figure 1. Boysenberry polyphenol ameliorates brown adipose tissue dysfunction

(A–E) Mice were fed a normal chow (NC) diet or high-fat diet (HFD) from 4 weeks of age for 17 weeks. Some HFD mice were given 0.1% boysenberry polyphenols (HFD + BoyP) through their drinking water also from 4 weeks of age.

(A) Hematoxylin and eosin (HE) staining of brown adipose tissue (BAT) of the indicated mice (scale bars = 100 μm). The right panel indicates the number of large lipid droplets (defined as droplets with a surface area >250 μm^2) per view (n = 4, 4, 4).

(B) BAT was weighed in the indicated groups (n = 11, 16, 16, excluding the outliers of n = 1, 1, 1).

(C) Results of quantitative polymerase chain reaction (qPCR) for *Ppargc1a* (n = 8, 10, 11, excluding the outlier of n = 1 in HFD) and *Ucp1* (n = 8, 10, 10, excluding the outlier of n = 2 in HFD + BoyP) in BAT.

(D) Results of glucose tolerance test (GTT, n = 6, 6, 6).

(E) Results of cold tolerance test (CTT) in a cold room at 4°C. The left panel shows the incidence of severe hypothermia (defined as a body temperature below 33°C), and the right panel shows raw body temperature data. (n = 9, 9, 9). (F-J) NC-fed mice were maintained under thermoneutral (TN; 30°C) or room temperature (RT; 24°C) conditions at age 11 to 15 weeks, and some mice were administered 0.1% BoyP in their drinking water.

(F) Images of HE staining of BAT and the number of large lipid droplets per view in the indicated groups (n = 4, 4, 4, excluding the outlier of n = 1 in RT). Scale bars = 100μm.

(G) BAT weight in RT, TN, and TN + BoyP mice (n = 8, 9, 9).

(H) qPCR studies for *Ppargc1a* (n = 11, 13, 13, excluding the outliers of n = 3 in TN) and *Ucp1* (n = 12, 12, 13, excluding the outliers of n = 1, 2, 1) in BAT.

(I) Results of GTT (n = 8, 9, 9).

(J) Results of CTT (n = 8, 14, 14). The left panel shows the incidence of severe hypothermia (defined as a body temperature below 33°C), and the right panel shows raw body temperature data. Data, where equal variances were assumed, were analyzed with one-way analysis of variance (ANOVA) followed by Tukey's multiple comparison test (A, B, F, and G) or repeated ANOVA followed by Tukey's multiple comparison test (D and I). Data, where equal variances were not assumed, were analyzed by Dunnett's T3 test (C and H). Data were analyzed by the log-rank test (E and J). *$p < 0.05$; **$p < 0.01$. Boxplots show the upper whisker, upper quartile, median, lower quartile, and lower whisker, and dots indicate raw data (A–C and F–H). Values represent the mean ± SD. (D and I). NS indicates that the difference was not significant. See also Figure S1.

depletion results in impaired angiogenesis and diastolic dysfunction in the left ventricle (Maizel et al., 2014). Endothelial inactivation of SIRT-1 also exhibits capillary rarefaction in the kidney (Kida et al., 2016), but the role of SIRT-1 in BAT capillarization is not known. Therefore, we studied the actions of boysenberry polyphenols (BoyP) in BAT. We found that the EC SIRT-1 pathway has a critical role in maintaining capillary network formation in BAT.

RESULTS

Polyphenols ameliorate brown adipose tissue dysfunction

To evaluate the biological effects of polyphenols in brown adipose tissue (BAT), 4-week-old male mice were fed a high-fat diet (HFD) and administered boysenberry polyphenols (BoyP) in their drinking water. Compared with BAT in normal chow (NC) mice, BAT in HFD mice showed whitening and had an increased tissue weight; both these characteristics were ameliorated by BoyP treatment (Figures 1A and 1B). The *Ppargc1a* gene encodes peroxisome proliferator-activated receptor gamma, a master regulator of mitochondrial biosynthesis. The *Ucp1* gene encodes uncoupling protein 1, a protein that plays a critical role in heat generation through non-shivering thermogenesis. These are known to be markers for BAT (Uldry et al., 2006), and we found the transcription of *Ppargc1a* and *Ucp1* was decreased in dietary obesity but increased with the introduction of BoyP (Figure 1C). Body weight, food, and water intake showed no significant differences between the HFD and HFD + BoyP groups (Figures S1A–S1C). HFD mice exhibited systemic glucose intolerance compared with NC mice, but BoyP administration ameliorated this intolerance in the dietary obesity model (Figure 1D). The thermogenic response under cold exposure was lower in the HFD group than in the NC group but increased with BoyP administration (Figure 1E). In the obesity model, BoyP also improved oxygen consumption (VO_2), CO_2 production (VCO_2), the respiratory exchange ratio (RER), and energy expenditure (EE; Figure S1D). In contrast, the administration of BoyP to NC mice did not affect the morphology of BAT (Figure S1E), body weight, BAT weight (Figures S1F and S1G), systemic glucose tolerance (Figure S1H), or thermogenic response (Figure S1I).

Next, we examined the effect of BoyP in another BAT dysfunction model. In general, mice are housed at a temperature of around 20°C to 22°C, a condition at which cold-induced activation of BAT is considered to develop; 29°C to 34°C is recognized as a thermoneutral temperature (TN) for mice (Vialard and Olivier, 2020). Studies found that mice maintained under TN conditions develop systemic glucose intolerance (Clayton and McCurdy, 2018), suppression of systemic lipid metabolism (Evangelakos et al., 2021), and BAT dysfunction (Cui et al., 2016). In NC mice, TN promoted BAT whitening and increased body or BAT weight, and both these effects were ameliorated by BoyP (Figures 1F, 1G, and S1J–S1L). The transcripts of *Ppargc1a* and *Ucp1* in BAT were reduced in the TN group but increased in the TN + BoyP group (Figure 1H). We also found that BoyP improved systemic glucose intolerance and increased the markers of

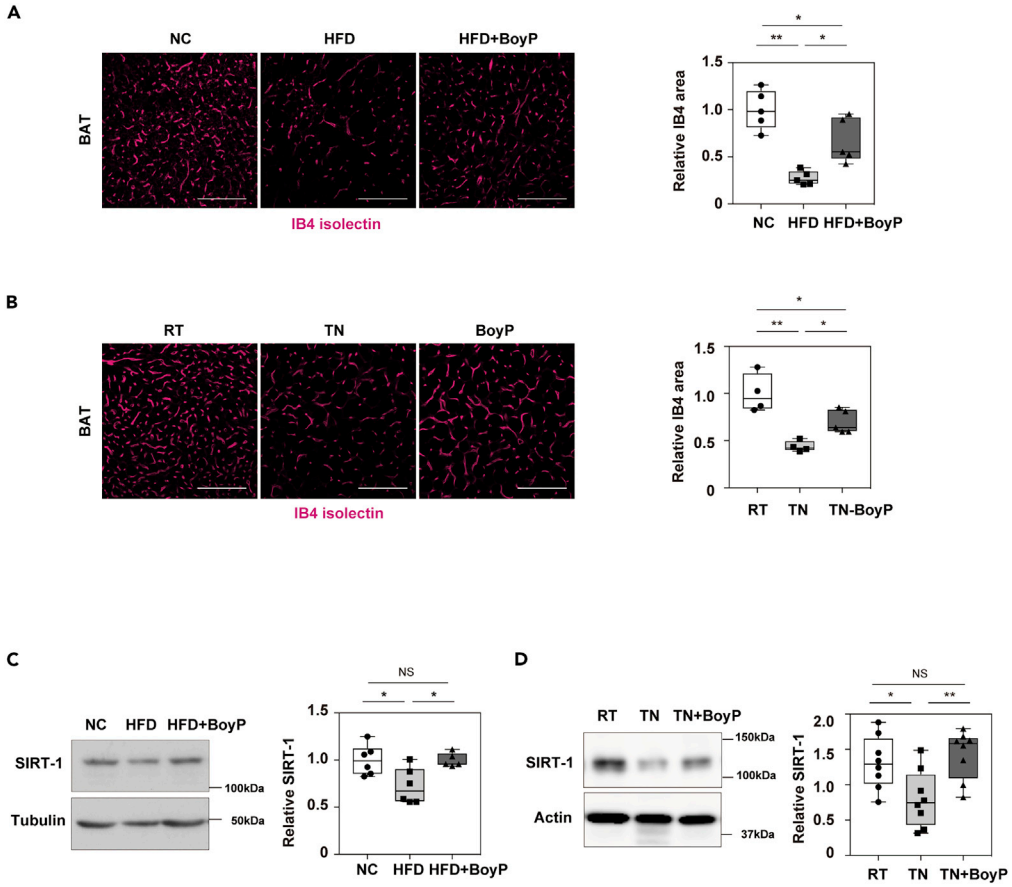

Figure 2. Boysenberry polyphenols suppress capillary rarefaction in brown adipose tissue

(A) Capillary network in brown adipose tissue (BAT) of normal chow (NC), high-fat diet (HFD), and HFD + boysenberry polyphenols (BoyP) mice were analyzed by IB4 isolectin immunofluorescence staining (scale bars = 100μm). The right panel indicates the relative area positive for IB4 (n = 5, 5, 5).

(B) Capillary network tested with IB4 isolectin immunostaining in BAT of room temperature (RT), thermoneutral (TN; 30°C), and TN + BoyP mice (scale bars = 100 μm). The right panel indicates the relative area positive for IB4 (n = 4, 4, 5).

(C and D) Western blot to test the level of Sirtuin-1 (SIRT-1), tubulin, and actin in the BAT of the indicated groups. The right panels show the quantification of SIRT-1 in the indicated groups compared with the respective controls (C: n = 4, 4, 4, excluding the outlier of n = 1 in HFD; D: n = 8, 8, 8). Data were analyzed with one-way analysis of variance followed by Tukey's multiple comparison test. *$p < 0.05$; **$p < 0.01$. Boxplots show the upper whisker, upper quartile, median, lower quartile, and lower whisker, and dots indicate raw data (A–D). NS indicates not significant. See also Figure S2.

systemic metabolism analyzed in metabolic cage studies (Figures 1I and S1M). The thermogenic response upon acute cold exposure was suppressed in the TN group, and this suppressed response was re-activated in the BoyP group (Figure 1J). These results suggest that BoyP enhances BAT activity and systemic metabolism in two models with BAT dysfunction.

Boysenberry polyphenols enhances capillarization in brown adipose tissue

We found that the capillary density was reduced in our dietary obesity model and that it increased with BoyP administration (Figure 2A). Introducing BoyP also enhanced capillary density in the BAT of mice maintained under thermoneutrality and fed an NC diet (Figure 2B). SIRT-1 is one of the main downstream molecules that mediate the biological effects of polyphenols (Price et al., 2012). Previous reports showed the role of SIRT-1 in capillarization in several organs, including heart and kidney (Das et al., 2018; Kida et al., 2016; Maizel et al., 2014). These findings led us to test the SIRT-1 level in the BAT of our models, and we found that SIRT-1 was reduced in BAT in the HFD and TN groups and that BoyP increased expression of this protein in both models (Figures 2C, 2D, S2A, and S2B). As a result of these studies, we considered that SIRT-1 was involved in mediating the biological effect of BoyP in our models.

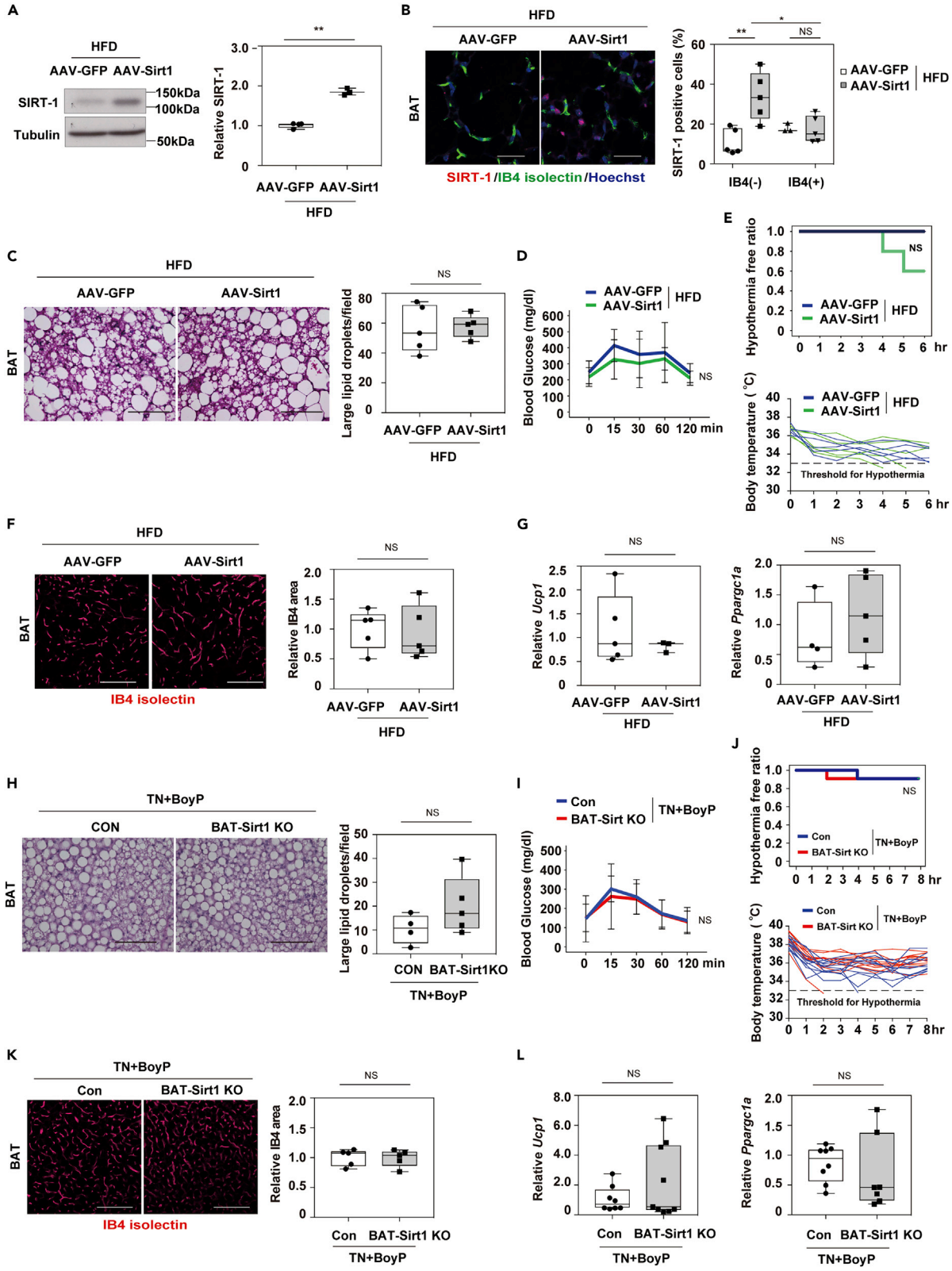
A
HFD
AAV-GFP AAV-Sirt1
SIRT-1
Tubulin
150kDa
100kDa
50kDa
Relative SIRT-1
AAV-GFP AAV-Sirt1
HFD
B
HFD
AAV-GFP
AAV-Sirt1
BAT
SIRT-1/IB4 isolectin/Hoechst
SIRT-1 positive cells (%)
IB4(-)
IB4(+)
AAV-GFP
AAV-Sirt1
HFD
C
HFD
AAV-GFP
AAV-Sirt1
BAT
Large lipid droplets/field
D
Blood Glucose (mg/dl)
120 min
E
Hypothermia free ratio
Body temperature (°C)
Threshold for Hypothermia
F
IB4 isolectin
Relative IB4 area
G
Relative Ucp1
Relative Ppargc1a
H
TN+BoyP
CON
BAT-Sirt1 KO
I
Con
BAT-Sirt KO
TN+BoyP
J
K
L
NS

Figure 3. Nicotinamide adenine dinucleotide -dependent protein deacetylase sirtuin 1 in brown adipocytes does not affect capillarization in brown adipose tissue

(A–G) Mice were fed a high-fat diet (HFD) from 4 to 22 weeks of age, and adeno-associated virus encoding *Sirt1* (AAV-*Sirt1*) was injected into brown adipose tissue (BAT) at 17 weeks of age.

(A) Western blot to test the level of nicotinamide adenine dinucleotide -dependent protein deacetylase sirtuin-1 (SIRT-1) in BAT of AAV-*Sirt1* and AAV-GFP groups. The right panel indicates the quantification of SIRT-1 compared with α-tubulin (n = 4, 3, excluding the outliers of n = 1, 2).

(B) Immunofluorescence staining to analyze SIRT-1 (red), IB4-isolectin (green), and nuclei (Hoechst; blue) in BAT of the indicated groups (scale bars = 50μm). SIRT-1-positive cells were counted in IB4-negative (−) or -positive (+) cells in the indicated groups (n = 5, 5, 3, 5, excluding the outliers of n = 2 for IB4(+) in AAV-GFP).

(C) Hematoxylin and eosin (HE) staining of BAT in the indicated groups (scale bars = 100 μm). The right panels show the number of large lipid droplets (defined as droplets with a surface area >250 μm^2) per field (n = 5, 5).

(D) Results of glucose tolerance test (GTT) (n = 5, 5).

(E) Cold tolerance test (CTT) (n = 5, 5) of the indicated groups. The upper panel shows the incidence of severe hypothermia (defined as a body temperature below 33°C), and the lower panel shows raw body temperature data.

(F) IB4-isolectin immunostaining image and relative area positive for IB4 (scale bars = 100 μm; n = 5, 5).

(G) Results of quantitative polymerase chain reaction (qPCR) for *Ppargc1a* (n = 4, 5 excluding the outlier of n = 1 in AAV-GFP) and *Ucp1* (n = 5, 3, excluding the outliers of n = 2 in AAV-Sirt1) in BAT of the indicated groups (n = 5, 5).

(H–L) BAT-specific *Sirt1* knockout mice (UCP-1 $Cre^{+/-}$; $Sirt1^{flox/flox}$; BAT-Sirt1 KO) were fed normal chow, maintained under thermoneutral conditions (30°C), and administered 0.1% BoyP in the drinking water.

(H) HE staining of BAT (scale bars = 100 μm) and number of large lipid droplets (defined as droplets with a surface area >250 μm^2) per field (n = 4, 5, excluding the outlier of n = 1 in WT).

(I) Results of GTT (n = 10, 11). (J) CTT (n = 11, 11) in the indicated groups. The upper panel shows the incidence of severe hypothermia (defined as a body temperature below 33°C), and the lower panel shows raw body temperature data.

(K) IB4-isolectin immunofluorescence staining and relative area positive for IB4 in the indicated groups (scale bars = 100 μm; n = 5, 5).

(L) Results of qPCR for *Ucp1* (n = 8, 9, excluding the outliers of n = 1, 1) and *Ppargc1a* (n = 8, 7, excluding the outliers of n = 2, 2) in BAT. Data were analyzed by two-tailed Student's *t* test (A, C, F, G, H, K, and L), one-way analysis of variance (ANOVA) followed by Tukey's multiple comparison test (B), repeated ANOVA (D and E), or the log-rank test (E and J). *p < 0.05; **p < 0.01. Boxplots show the upper whisker, upper quartile, median, lower quartile, and lower whisker, and dots indicate raw data (A–C, F–H, K, and L). Values represent the mean ± SD. (D and I). NS indicates not significant. See also Figure S3.

Sirtuin 1 in brown adipocytes does not regulate capillarization in brown adipose tissue

To further test the role of SIRT-1 in BAT, we generated an obesity model with overexpression of SIRT-1 in BAT. To do so, we directly injected adeno-associated virus (AAV) encoding *Sirt1* into the BAT of mice fed a HFD (AAV-*Sirt1* HFD). This AAV-*Sirt1* HFD model showed a higher level of SIRT-1 in BAT than the AAV-GFP group did (Figures 3A and S3A). Although SIRT-1 expression did not increase in endothelial cells (ECs), it did increase in other cell components (Figure 3B). AAV-*Sirt1* HFD and AAV-GFP HFD mice showed no marked differences in BAT histology (Figure 3C), body or BAT weight (Figures S3B and S3C), systemic glucose intolerance (Figure 3D), and thermogenic response to 8 h-acute cold exposure (Figure 3E). In addition, no significant differences in capillary density (Figure 3F) or transcripts *Ucp1* or *Ppargc1a* (Figure 3G) were found between the AAV-GFP and AAV-*Sirt1* groups.

Next, we generated a BAT-specific *Sirt1* knockout (KO) model by crossing UCP-1 $Cre^{+/-}$ with $Sirt1^{flox/flox}$ mice (BAT-*Sirt1* KO). The level of SIRT-1 was significantly reduced in the BAT-*Sirt1* KO mice fed a NC diet (Figures S3D and S3E). We characterized the phenotypes of these mice in the TN model and found no marked difference between the genotypes in BAT histology (Figure 3H), body or BAT weight (Figures S3F and S3G), systemic glucose intolerance (Figure 3I), thermogenic response (Figure 3J), capillary density (Figure 3K), or transcripts *Ucp1* or *Ppargc1a* (Figure 3L). These results suggested that SIRT-1 in brown adipocytes has minor roles for capillarization in BAT.

Characterization of endothelial cell sirtuin 1 and endothelial cell apoptosis in brown adipose tissue

EC SIRT-1 was reported to increase capillary density in aged skeletal muscle (Li et al., 2022), and in the retina, activation of SIRT-1 was shown to prevent reactive oxygen species-induced apoptosis in ECs (Li et al., 2017). We found that the EC SIRT-1 level decreased with dietary obesity and increased with BoyP administration (Figures 4A, 4B, and S4A). As mentioned above, angiogenesis/vasculogenesis and apoptosis of ECs regulate capillarization in organs (Grant et al., 2020; Korn and Augustin, 2015). The number of apoptotic cells in ECs was increased with a HFD and decreased with BoyP administration (Figure 4C). In our TN model, we found also a reduction in EC SIRT-1, which increased with the introduction of BoyP (Figures 4D, 4E, and S4B). EC apoptosis was increased in thermoneutrality and reduced with BoyP administration (Figure 4F). These results suggested a potential role of EC SIRT-1 in the regulation of EC apoptosis and capillary network formation in BAT.

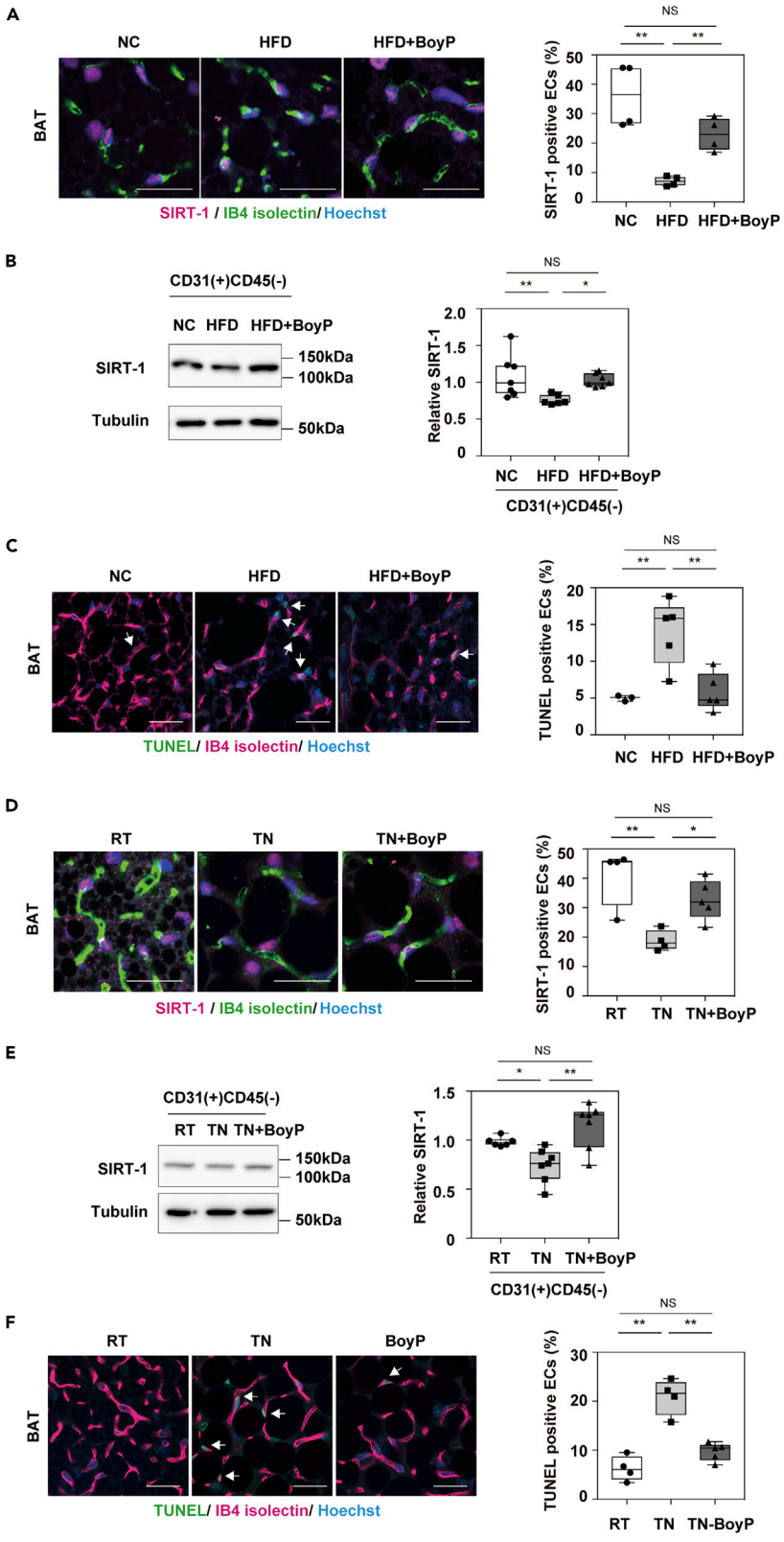
A
NC
HFD
HFD+BoyP
BAT
SIRT-1 / IB4 isolectin/ Hoechst
NS
**
**
SIRT-1 positive ECs (%)
50
40
30
20
10
0
NC HFD HFD+BoyP
B
CD31(+)CD45(-)
NC HFD HFD+BoyP
SIRT-1
150kDa
100kDa
Tubulin
50kDa
NS
**
*
Relative SIRT-1
2.0
1.5
1.0
0.5
0
NC HFD HFD+BoyP
CD31(+)CD45(-)
C
NC
HFD
HFD+BoyP
BAT
TUNEL/ IB4 isolectin/ Hoechst
NS
**
**
TUNEL positive ECs (%)
20
15
10
5
0
NC HFD HFD+BoyP
D
RT
TN
TN+BoyP
BAT
SIRT-1 / IB4 isolectin/ Hoechst
NS
**
*
SIRT-1 positive ECs (%)
50
40
30
20
10
0
RT TN TN+BoyP
E
CD31(+)CD45(-)
RT TN TN+BoyP
SIRT-1
150kDa
100kDa
Tubulin
50kDa
NS
*
**
Relative SIRT-1
1.5
1.0
0.5
0
RT TN TN+BoyP
CD31(+)CD45(-)
F
RT
TN
BoyP
BAT
TUNEL/ IB4 isolectin/ Hoechst
NS
**
**
TUNEL positive ECs (%)
30
20
10
0
RT TN TN-BoyP

Figure 4. Boysenberry polyphenols enhanced nicotinamide adenine dinucleotide-dependent protein deacetylase sirtuin 1 expression and suppressed apoptosis in endothelial cells of brown adipose tissue

Mice were fed a normal chow (NC) diet or high fat diet (HFD) from 4 weeks of age for 17 weeks. Some HFD mice were given 0.1% boysenberry polyphenols (HFD + BoyP) through their drinking water from 4 weeks of age.

(A) Immunofluorescence staining to analyze nicotinamide adenine dinucleotide-dependent protein deacetylase sirtuin 1 (SIRT-1; red), IB4-isolectin (green), and nuclei (Hoechst; blue) in brown adipose tissue (BAT) of the indicated groups (scale bars = 50 μm). The right panel indicates the ratio of SIRT-1–positive endothelial cells (ECs; n = 4, 4, 4).

(B) Western blot study to analyze SIRT-1 in CD31(+) CD45(-) cells of BAT. The right panel indicates the relative SIRT-1 level compared with the tubulin loading control (n = 6, 7, 7, excluding the outlier of n = 1 in NC).

(C) Immunofluorescence staining to analyze terminal deoxynucleotidyl transferase-mediated dUTP nick end labeling (TUNEL; green), ECs (IB4-isolectin, red) and nuclei (Hoechst; blue) in the indicated groups (scale bars = 50 μm). The right panel indicates TUNEL-positive ECs (%; n = 3, 5, 5, excluding the outliers of n = 2 in NC).

(D) Immunofluorescence staining of SIRT-1 (red), ECs (IB4-isolectin, green), and nuclei (Hoechst; blue) in BAT of the indicated mice fed NC (scale bars = 50 μm). The right panel indicates SIRT-1–positive ECs (%; n = 4, 4, 5).

(E) Western blot analyses to detect SIRT-1 and tubulin levels in CD31(+) CD45(-) cells from BAT of the indicated mice fed NC (n = 6, 7, 7, excluding the outliers of n = 1 in RT). The right panel indicates the quantification of SIRT-1 against the tubulin loading control.

(F) Immunofluorescence staining to analyze TUNEL (green), ECs (IB4-isolectin, red), and nuclei (Hoechst; blue) of the indicated mice fed NC (scale bars = 50 μm). The right panel indicates TUNEL-positive ECs (%; n = 4, 4, 5). Data were analyzed with one-way analysis of variance followed by Tukey's multiple comparison test. *$p < 0.05$; **$p < 0.01$. Boxplots show the upper whisker, upper quartile, median, lower quartile, and lower whisker, and dots indicate raw data (A-F). NS indicates not significant. See also Figure S4.

Endothelial cell sirtuin 1 depletion abolishes the effect of boysenberry polyphenols in brown adipose tissue

To further test the role of EC SIRT-1, we generated EC-specific *Sirt1*-KO mice by crossing VEcadherin-BAC-CreERT2 (Okabe et al., 2014) with *Sirt1*$^{flox/flox}$ mice (EC-*Sirt1* KO; Figures 5A and S5A). These models showed no significant differences in systemic glucose tolerance or thermogenic capacity when maintained at room temperature (Figures S5B and S5C). We maintained these mice under TN conditions and administered BoyP (TN + BoyP) and found that EC-*Sirt1* KO mice exhibited a whitened phenotype of BAT compared with littermate control mice (Figure 5B). Under this condition, EC-*Sirt1* KO model mice showed also reduced capillary density (Figure 5C) and UCP-1 levels (Figures 5D and S5D) in BAT, enhanced systemic glucose intolerance (Figure 5E), and suppressed thermogenic capacity (Figure 5F). Body and BAT weight were comparable between the genotypes (Figures S5E and S5F). The number of ECs positive for terminal deoxynucleotidyl transferase-mediated dUTP nick end labeling (TUNEL) also increased in the EC-*Sirt1* KO model (Figure 5G).

As already described, housing mice under TN conditions leads to suppression of systemic lipid metabolism, and the levels of triglyceride and free fatty acid were reported to increase with thermoneutrality (Evangelakos et al., 2021; Labbe et al., 2016). Similar to a previous study (Wang et al., 2021), in our study, the administration of palmitic acid-induced apoptosis in human umbilical vein endothelial cells (HUVECs), and co-administration of BoyP suppressed this apoptosis (Figure 5H). We also found that the anti-apoptotic effect of BoyP diminished with the introduction of a SIRT-1 inhibitor (Figure 5H). Resveratrol is reported to activate SIRT-1 through allosteric activation (Hubbard et al., 2013). We next sought to test the direct effect of BoyP on SIRT-1 activity. The tumor suppressor protein p53 promotes apoptosis (Aubrey et al., 2018) and is known to be activated by the acetylation of Lys382 (Lys379 in mouse) (Sakaguchi et al., 1998). Deacetylation of p53 occurs through interaction with SIRT-1 (Solomon et al., 2006). We found that palmitic acid-induced acetylation of p53 in HUVECs and that the addition of BoyP significantly decreased acetyl-p53 levels (Figures 5I and S5G). To further test whether BoyP directly activates SIRT-1, we measured SIRT-1 enzyme activity *in vitro* and found that BoyP promoted the deacetylation of fluoro-substrate peptide by recombinant SIRT-1 (Figure S5H), suggesting that BoyP directly activates SIRT-1. The main constituent of BoyP is anthocyanin (BoyAC) (Furuuchi et al., 2011), and previously, BoyAC was obtained from column fractionation and tested in studies with HUVECs (Furuuchi et al., 2018). We found that the introduction of BoyAC ameliorated palmitic acid-induced apoptosis in HUVECs and that this anti-apoptotic effect was suppressed by a SIRT-1 inhibitor (Figure S5I).

Taken together, our results suggest that EC SIRT1 plays a role in BAT capillarization and that the activation of EC SIRT1 would be one of the potential mechanisms that mediate the effects of BoyP treatment on BAT homeostasis.

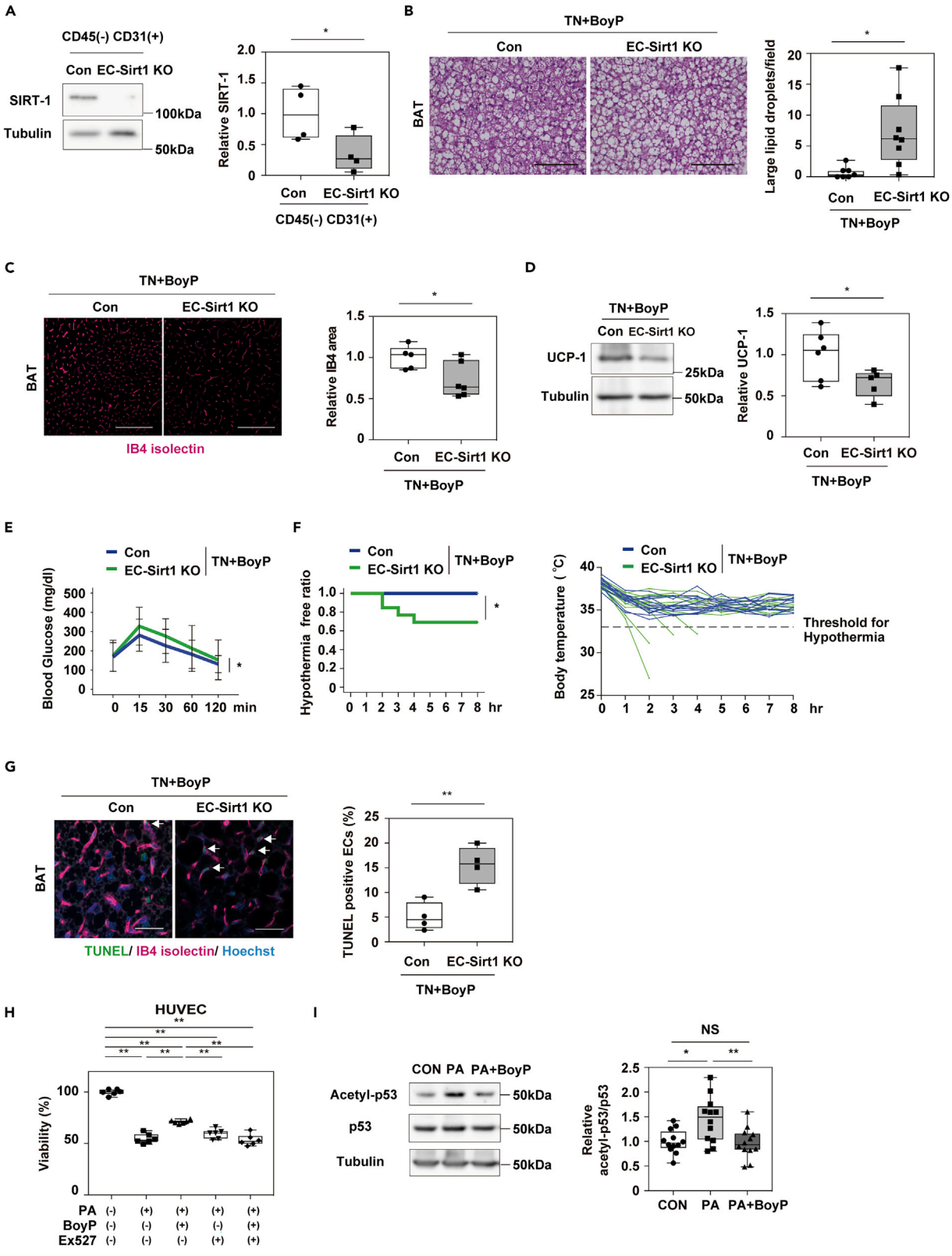
A
CD45(-) CD31(+)
Con EC-Sirt1 KO
SIRT-1
Tubulin
100kDa
50kDa
Relative SIRT-1
Con EC-Sirt1 KO
CD45(-) CD31(+)
B
TN+BoyP
Con
EC-Sirt1 KO
BAT
Large lipid droplets/field
Con EC-Sirt1 KO
TN+BoyP
C
TN+BoyP
Con
EC-Sirt1 KO
BAT
IB4 isolectin
Relative IB4 area
Con EC-Sirt1 KO
TN+BoyP
D
TN+BoyP
Con EC-Sirt1 KO
UCP-1
Tubulin
25kDa
50kDa
Relative UCP-1
Con EC-Sirt1 KO
TN+BoyP
E
Con
EC-Sirt1 KO
TN+BoyP
Blood Glucose (mg/dl)
0 15 30 60 120 min
F
Con
EC-Sirt1 KO
TN+BoyP
Hypothermia free ratio
0 1 2 3 4 5 6 7 8 hr
Con
EC-Sirt1 KO
TN+BoyP
Body temperature (°C)
Threshold for Hypothermia
0 1 2 3 4 5 6 7 8 hr
G
TN+BoyP
Con
EC-Sirt1 KO
BAT
TUNEL/ IB4 isolectin/ Hoechst
TUNEL positive ECs (%)
Con EC-Sirt1 KO
TN+BoyP
H
HUVEC
Viability (%)
PA (-) (+) (+) (+) (+)
BoyP (-) (-) (+) (-) (+)
Ex527 (-) (-) (-) (+) (+)
I
CON PA PA+BoyP
Acetyl-p53
p53
Tubulin
50kDa
50kDa
50kDa
NS
Relative acetyl-p53/p53
CON PA PA+BoyP

Figure 5. Depletion of nicotinamide adenine dinucleotide-dependent protein deacetylase sirtuin 1 in endothelial cells abolished effect of boysenberry polyphenols in brown adipose tissue

VEcadherin-BAC-CreERT2$^{+/-}$; *Sirt1*$^{flox/flox}$ (endothelial cell [EC]-*Sirt1* knockout [KO]) and VEcadherin-BAC-CreERT2$^{-/-}$; *Sirt1*$^{flox/flox}$ (Con) mice were fed normal chow (NC), maintained under thermoneutral (TN) conditions (30℃) and administered 0.1% boysenberry polyphenols (BoyP) in their drinking water (TN + BoyP) from 11 to 17 weeks of age. At 13 weeks of age, these mice were subjected to further analyses.

(A) Western blot to analyze expression of SIRT-1 in CD45(-) CD31(+) cells of brown adipose tissue (BAT) in indicated groups fed NC under room temperature (n = 4, 4).

(B) Hematoxylin and eosin staining of BAT in indicated groups under TN + BoyP conditions (scale bars = 100 μm). The right panel indicates the number of large lipid droplets (defined as droplets with a surface area > 250 μm^2) per view (n = 8, 9, excluding the outliers of n = 1, 1).

(C) Capillary network analyzed with IB4-isolectin immunofluorescence staining (scale bars = 100 μm). The right panel indicates the relative area positive for IB4 (n = 5, 6).

(D) Western blot to analyze UCP-1 in BAT of the indicated groups (n = 6, 6).

(E) Results of glucose tolerance test (n = 15, 13).

(F) Results of cold tolerance test (n = 14, 13). The left panel shows the incidence of severe hypothermia (defined as a body temperature below 33℃), and the right panel shows raw body temperature data.

(G) Apoptosis of IB4-positive cells were analyzed by terminal deoxynucleotidyl transferase-mediated dUTP nick end labeling (TUNEL) staining (scale bars = 50 μm). The right panel indicates TUNEL-positive ECs in the indicated groups (n = 4, 4).

(H) 3-(4,5-dimethyl-2-thiazolyl)-2,5-diphenyl-2H-tetrazolium bromide (MTT) assay to analyze the viability of human umbilical vein endothelial cells under the following conditions: 100 μM palmitic acid, 1 μg/mL BoyP, and 10 μM Ex527 (a SIRT-1 inhibitor; n = 6, 6, 6, 6, 6).

(I) Western blot analyses for the levels of Acetyl-p53, p53, and tubulin in human umbilical vein endothelial cells (HUVEC) treated with 100 μM palmitic acid 1 μg/mL ± BoyP for 24 hours. The right panels show quantification of acetyl-p53/p53 in the indicated groups compared with the respective controls (n = 12, 12, 12). Data were analyzed by the two-tailed Student's *t* test (A, B, C, D and G), one-way analysis of variance (ANOVA) followed by Tukey's multiple comparison test (H, I), repeated ANOVA (E), or log rank test (F). *p < 0.05; **p < 0.01. Boxplots show the upper whisker, upper quartile, median, lower quartile, and lower whisker, and dots indicate raw data (A-D, G-I). Values represent the mean ± SD. (E). NS indicates not significant. See also Figure S5.

DISCUSSION

Oxygen and nutrients are delivered through capillaries, and this platform has a critical role in maintaining organ function. With aging and age-related disorders, capillary rarefaction develops in tissues, including heart and BAT, and this development is considered to have a causal role in the progression of functional decline in these organs (Grunewald et al., 2021; Shimizu et al., 2014). Accumulating evidence shows that BAT has critical roles in maintaining systemic metabolic health (Bartelt et al., 2011; Stanford et al., 2013; Yoneshiro et al., 2013). In dietary obese mice, implantation of BAT decreased body weight and improved systemic glucose intolerance (Stanford et al., 2013). Activation of BAT was shown to reduce the weight of adipose tissue in humans (Yoneshiro et al., 2013). Previously, we reported that dietary obesity diminished the capillary density in BAT of obese mice (Shimizu et al., 2014). Mechanistically, the excessive influx of free fatty acid into brown adipocytes reduced VEGF-A production in these cells (Shimizu et al., 2014). Adipose-*Vegfa* KO mice maintained on an NC diet exhibited a whitened phenotype of BAT, systemic glucose intolerance, and a reduced thermogenic response (Shimizu et al., 2014). Capillarization is regulated through the balance between angiogenesis/vasculogenesis and apoptosis of ECs (Grant et al., 2020; Korn and Augustin, 2015). To explore an anti-apoptotic mechanism of ECs in BAT, we analyzed a polyphenol administration model in which we tested BoyP, the polyphenols available in our lab. Polyphenols are reported to activate BAT function, but the underlying mechanisms remain to be explored. Boysenberry, the source of BoyP, is a berry rich in polyphenols, mainly anthocyanins, ellagic acid, and ellagitannins (Furuuchi et al., 2011). BoyP were reported to decrease the level of reactive oxygen species and have a protective effect on vascular endothelial function (Furuuchi et al., 2018; Matsushima et al., 2014).

We generated two BAT dysfunction models: 1) mice maintained on a HFD at room temperature, 2) mice maintained on NC at a TN temperature. In both of these models, the capillary density in BAT was reduced and administration of BoyP enhanced capillarization in BAT and induced re-browning of BAT. These changes were associated with an increase in thermogenic capacity and amelioration of systemic glucose intolerance. To further clarify the underlying mechanisms, we focused on testing the potential role of SIRT-1 in mediating the biological effect of BoyP. SIRT-1 is well known to be activated by polyphenols (Shakibaei et al., 2011), and studies indicated that it has roles in maintaining capillarization in kidney and heart (Kida et al., 2016; Maizel et al., 2014). We found that BoyP increased SIRT-1 in the BAT of our animal models.

Next, we generated *Sirt1* overexpression and BAT-specific *Sirt1* depletion models. Interestingly, gain or loss of SIRT-1 in brown adipocytes did not lead to a change in histological findings in BAT or in capillarization in this organ. In our BAT dysfunctional models, the level of EC SIRT-1 was reduced and apoptosis in these cells was increased. These findings led us to test the role of SIRT-1 in ECs. We generated an EC

Sirt1 KO model and tested its phenotype under thermoneutrality. Mice were maintained under TN conditions and administered BoyP. Compared with the littermate control mice, EC-*Sirt1* KO mice exhibited a marked whitened phenotype in BAT. In addition, they showed also reduced capillary density and enhanced EC apoptosis. These changes were associated with systemic glucose intolerance and reduced thermogenic capacity, suggesting that EC SIRT-1 has critical roles in maintaining capillarization in BAT and in systemic glucose metabolism.

Limitations of the study

This was a preclinical study, so human trials are needed to evaluate the effects of BoyP in humans. Since BoyP is derived from the juice of cultivated boysenberries, the concentration of polyphenol content including BoyAC varies among particular years as indicated in the Methods. Dietary obese mice, thermoneutral mice, and EC or BAT SIRT-1 KO mice were tested by administering BoyP in drinking water, so a potential systemic effect cannot be excluded. We tested an EC-specific *Sirt1* KO model, but we did not generate and analyze EC-specific *Sirt1* gain-of-function transgenic mice. Only male mice were used in this study, and a potential difference between genders remains to be explored. This study tested only a high-fat diet fed mouse model and did not analyze non-diet-induced obese models. We have not identified specific contents that contribute to the beneficial effects of BoyP, and these contents may also interact with many other proteins outside of SIRT1.

STAR★METHODS

Detailed methods are provided in the online version of this paper and include the following:

- KEY RESOURCES TABLE
- RESOURCE AVAILABILITY
  - Lead contact
  - Materials availability
  - Data and code availability
- EXPERIMENTAL MODEL AND SUBJECT DETAILS
  - Animal models
- METHOD DETAILS
  - Boysenberry polyphenols
  - Isolation of ECs
  - Glucose tolerance test
  - Cold tolerance test
  - Plasma insulin level
  - Histological analysis
  - RNA analysis
  - Respiratory gas analysis
  - Western blot analysis
  - Cell culture and viability test
  - Adeno-associated virus
  - SIRT-1 activity analysis
- QUANTIFICATION AND STATISTICAL ANALYSIS
  - Statistical analysis

SUPPLEMENTAL INFORMATION

Supplemental information can be found online at https://doi.org/10.1016/j.isci.2022.105424.

ACKNOWLEDGMENTS

We thank Evan Rosen at Harvard Medical School for providing the Ucp-Cre mice. This work was supported by a Grant-in-Aid for Scientific Research (A) (20H00533) and Grant-in-Aid for Challenging Research (Pioneering) (22K18389) from MEXT, AMED under Grant Number JP20ek0210114, and AMED-CREST under Grant Number JP20gm1110012, and Moonshot Research and Development Program (21zf0127003s0201), MEXT Supported Program for the Scleroderma Research Foundation at Private Universities Japan, Private University Research Branding Project, and Leading Initiative for Excellent Young Researchers, and grants from the Science Research Promotion Fund, the Takeda Medical Research

Foundation, the Vehicle Racing Commemorative Foundation, Ono Medical Research Foundation, and the Suzuken Memorial Foundation (to T.M.), a Grant-in-Aid for Scientific Research (C) (19K08485; to R.F.), the AMED Project for Elucidating and Controlling Mechanisms of Aging and Longevity under Grant Number JP21gm5010002, Fusion Oriented REsearch for disruptive Science and Technology under Grant Number JPMJFR200L (JST FOREST Program; to I.S.), and by a grant from Bourbon Corporation (to T.M., I.S., and Y.Y.).

AUTHOR CONTRIBUTIONS

I.S. and T.M. designed the study and wrote the article. R.F. and I.S. performed most of the experiments. Y.Y., M.S., and G.K. performed the *in vivo* study. Y.K. and K.W. contributed to mouse studies.

DECLARATION OF INTERESTS

R.F. is a member of Bourbon Corporation; however, this company did not play any role in the study design, data collection, and analysis, decision to publish, or preparation of the article and only provided financial support in the form of the author's salary and research materials. None of the other authors has a conflict of interest to declare.

Received: April 11, 2022
Revised: September 6, 2022
Accepted: October 18, 2022
Published: November 18, 2022

REFERENCES

Aubrey, B.J., Kelly, G.L., Janic, A., Herold, M.J., and Strasser, A. (2018). How does p53 induce apoptosis and how does this relate to p53-mediated tumour suppression? Cell Death Differ. *25*, 104–113.

Bartelt, A., Bruns, O.T., Reimer, R., Hohenberg, H., Ittrich, H., Peldschus, K., Kaul, M.G., Tromsdorf, U.I., Weller, H., Waurisch, C., et al. (2011). Brown adipose tissue activity controls triglyceride clearance. Nat. Med. *17*, 200–U293.

Becher, T., Palanisamy, S., Kramer, D.J., Eljalby, M., Marx, S.J., Wibmer, A.G., Butler, S.D., Jiang, C.S., Vaughan, R., Schöder, H., et al. (2021). Brown adipose tissue is associated with cardiometabolic health. Nat. Med. *27*, 58–65.

Clayton, Z.S., and McCurdy, C.E. (2018). Short-term thermoneutral housing alters glucose metabolism and markers of adipose tissue browning in response to a high-fat diet in lean mice. Am. J. Physiol. Regul. Integr. Comp. Physiol. *315*, R627–R637.

Cui, X., Nguyen, N.L.T., Zarebidaki, E., Cao, Q., Li, F., Zha, L., Bartness, T., Shi, H., and Xue, B. (2016). Thermoneutrality decreases thermogenic program and promotes adiposity in high-fat diet-fed mice. Physiol. Rep. *4*, e12799.

Das, A., Huang, G.X., Bonkowski, M.S., Longchamp, A., Li, C., Schultz, M.B., Kim, L.J., Osborne, B., Joshi, S., Lu, Y., et al. (2018). Impairment of an endothelial NAD(+)-H2S signaling network is a reversible cause of vascular aging. Cell *173*, 74–89.e20.

Després, J.P., Carpentier, A.C., Tchernof, A., Neeland, I.J., and Poirier, P. (2021). Management of obesity in cardiovascular practice JACC focus seminar. J. Am. Coll. Cardiol. *78*, 513–531.

Evangelakos, I., Schwinge, D., Worthmann, A., John, C., Roeder, N., Pertzborn, P., Behrens, J., Schramm, C., Scheja, L., and Heeren, J. (2021). Oxysterol 7-alpha hydroxylase (CYP7B1) attenuates metabolic-associated fatty liver disease in mice at thermoneutrality. Cells *10*, 2656.

Furuuchi, R., Shimizu, I., Yoshida, Y., Hayashi, Y., Ikegami, R., Suda, M., Katsuumi, G., Wakasugi, T., Nakao, M., and Minamino, T. (2018). Boysenberry polyphenol inhibits endothelial dysfunction and improves vascular health. PLoS One *13*, e0202051.

Furuuchi, R., Yokoyama, T., Watanabe, Y., and Hirayama, M. (2011). Identification and quantification of short oligomeric proanthocyanidins and other polyphenols in boysenberry seeds and juice. J. Agric. Food Chem. *59*, 3738–3746.

Grant, Z.L., Whitehead, L., Wong, V.H., He, Z., Yan, R.Y., Miles, A.R., Benest, A.V., Bates, D.O., Prahst, C., Bentley, K., et al. (2020). Blocking endothelial apoptosis revascularizes the retina in a model of ischemic retinopathy. J. Clin. Invest. *130*, 4235–4251.

Grunewald, M., Kumar, S., Sharife, H., Volinsky, E., Gileles-Hillel, A., Licht, T., Permyakova, A., Hinden, L., Azar, S., Friedmann, Y., et al. (2021). Counteracting age-related VEGF signaling insufficiency promotes healthy aging and extends life span. Science *373*, eabc8479.

Hubbard, B.P., Gomes, A.P., Dai, H., Li, J., Case, A.W., Considine, T., Riera, T.V., Lee, J.E., Yen, E.S., Lamming, D.W., et al. (2013). Evidence for a common mechanism of SIRT1 regulation by allosteric activators. Science *339*, 1216–1219.

Kida, Y., Zullo, J.A., and Goligorsky, M.S. (2016). Endothelial sirtuin 1 inactivation enhances capillary rarefaction and fibrosis following kidney injury through Notch activation. Biochem. Biophys. Res. Commun. *478*, 1074–1079.

Korn, C., and Augustin, H.G. (2015). Mechanisms of vessel pruning and regression. Dev. Cell *34*, 5–17.

Kuryłowicz, A., and Puzianowska-Kuźnicka, M. (2020). Induction of adipose tissue browning as a strategy to combat obesity. Int. J. Mol. Sci. *21*, E6241.

Labbé, S.M., Caron, A., Chechi, K., Laplante, M., Lecomte, R., and Richard, D. (2016). Metabolic activity of brown, "beige, " and white adipose tissues in response to chronic adrenergic stimulation in male mice. Am. J. Physiol. Endocrinol. Metab. *311*, E260–E268.

Li, J., Yu, S., Ying, J., Shi, T., and Wang, P. (2017). Resveratrol prevents ROS-induced apoptosis in high glucose-treated retinal capillary endothelial cells via the activation of AMPK/Sirt1/PGC-1alpha pathway. Oxid. Med. Cell. Longev. *2017*, 7584691.

Li, J., Zhang, Y., Zeng, X., Cheng, Y., Tang, L., Hong, D., and Yang, X. (2022). Lycopene ameliorates insulin resistance and increases muscle capillary density in aging via activation of SIRT1. J. Nutr. Biochem. *99*, 108862.

van Marken Lichtenbelt, W.D., Vanhommerig, J.W., Smulders, N.M., Drossaerts, J.M.A.F.L., Kemerink, G.J., Bouvy, N.D., Schrauwen, P., and Teule, G.J.J. (2009). Cold-activated Brown adipose tissue in healthy men. N. Engl. J. Med. *360*, 1500–1508.

Lynes, M.D., Leiria, L.O., Lundh, M., Bartelt, A., Shamsi, F., Huang, T.L., Takahashi, H., Hirshman, M.F., Schlein, C., Lee, A., et al. (2017). The cold-induced lipokine 12, 13-diHOME promotes fatty acid transport into brown adipose tissue. Nat. Med. *23*, 1384.

Maizel, J., Xavier, S., Chen, J., Lin, C.H.S., Vasko, R., and Goligorsky, M.S. (2014). Sirtuin 1 ablation

in endothelial cells is associated with impaired angiogenesis and diastolic dysfunction. Am. J. Physiol. Heart Circ. Physiol. *307*, H1691–H1704.

Matsushima, A., Furuuchi, R., Shirai, M., Nagai, S., Yokoyama, T., Nishida, H., and Hirayama, M. (2014). Effects of acute and chronic boysenberry intake on blood pressure and endothelial function in spontaneous hypertensive rats. J. Nutr. Sci. Vitaminol. *60*, 43–51.

Milton-Laskibar, I., Aguirre, L., Etxeberria, U., Milagro, F.I., Martínez, J.A., and Portillo, M.P. (2018). Do the effects of resveratrol on thermogenic and oxidative capacities in IBAT and skeletal muscle depend on feeding conditions? Nutrients *10*, E1446.

Okabe, K., Kobayashi, S., Yamada, T., Kurihara, T., Tai-Nagara, I., Miyamoto, T., Mukouyama, Y.S., Sato, T.N., Suda, T., Ema, M., and Kubota, Y. (2014). Neurons limit angiogenesis by titrating VEGF in retina. Cell *159*, 584–596.

Plumb, J.A. (1999). Cell sensitivity assays: the MTT assay. Methods Mol. Med. *28*, 25–30.

Price, N.L., Gomes, A.P., Ling, A.J.Y., Duarte, F.V., Martin-Montalvo, A., North, B.J., Agarwal, B., Ye, L., Ramadori, G., Teodoro, J.S., et al. (2012). SIRT1 is required for AMPK activation and the beneficial effects of resveratrol on mitochondrial function. Cell Metabol. *15*, 675–690.

Rosen, E.D., and Spiegelman, B.M. (2014). What we talk about when we talk about fat. Cell *156*, 20–44.

Sakaguchi, K., Herrera, J.E., Saito, S., Miki, T., Bustin, M., Vassilev, A., Anderson, C.W., and Appella, E. (1998). DNA damage activates p53 through a phosphorylation-acetylation cascade. Genes Dev. *12*, 2831–2841.

Scheja, L., and Heeren, J. (2019). The endocrine function of adipose tissues in health and cardiometabolic disease. Nat. Rev. Endocrinol. *15*, 507–524.

Schneider, C.A., Rasband, W.S., and Eliceiri, K.W. (2012). NIH Image to ImageJ: 25 years of image analysis. Nat. Methods *9*, 671–675.

Shakibaei, M., Buhrmann, C., and Mobasheri, A. (2011). Resveratrol-mediated SIRT-1 interactions with p300 modulate receptor activator of NF-kappa B ligand (RANKL) activation of NF-kappa B signaling and inhibit osteoclastogenesis in bone-derived cells. J. Biol. Chem. *286*, 11492–11505.

Shimizu, I., Aprahamian, T., Kikuchi, R., Shimizu, A., Papanicolaou, K.N., MacLauchlan, S., Maruyama, S., and Walsh, K. (2014). Vascular rarefaction mediates whitening of brown fat in obesity. J. Clin. Invest. *124*, 2099–2112.

Solomon, J.M., Pasupuleti, R., Xu, L., McDonagh, T., Curtis, R., DiStefano, P.S., and Huber, L.J. (2006). Inhibition of SIRT1 catalytic activity increases p53 acetylation but does not alter cell survival following DNA damage. Mol. Cell Biol. *26*, 28–38.

Stanford, K.I., Middelbeek, R.J.W., Townsend, K.L., An, D., Nygaard, E.B., Hitchcox, K.M., Markan, K.R., Nakano, K., Hirshman, M.F., Tseng, Y.H., and Goodyear, L.J. (2013). Brown adipose tissue regulates glucose homeostasis and insulin sensitivity. J. Clin. Invest. *123*, 215–223.

Stucker, S., De Angelis, J., and Kusumbe, A.P. (2021). Heterogeneity and dynamics of vasculature in the endocrine system during aging and disease. Front. Physiol. *12*, 624928.

Uldry, M., Yang, W.L., St-Pierre, J., Lin, J.D., Seale, P., and Spiegelman, B.M. (2006). Complementary action of the PGC-1 coactivators in mitochondrial biogenesis and brown fat differentiation (vol 3, pg 333, 2006). Cell Metabol. *4*, 97.

Vialard, F., and Olivier, M. (2020). Thermoneutrality and immunity: how does cold stress affect disease? Front. Immunol. *11*, 588387.

Wang, M., Liu, F., Fang, B., Huo, Q., and Yang, Y. (2021). Proteome-scale profiling reveals MAFF and MAFG as two novel key transcription factors involved in palmitic acid-induced umbilical vein endothelial cell apoptosis. BMC Cardiovasc. Disord. *21*, 448.

Wang, S., Liang, X., Yang, Q., Fu, X., Zhu, M., Rodgers, B.D., Jiang, Q., Dodson, M.V., and Du, M. (2017). Resveratrol enhances brown adipocyte formation and function by activating AMP-activated protein kinase (AMPK) alpha 1 in mice fed high-fat diet. Mol. Nutr. Food Res. *61*, 1600746.

Yokoyama, M., Okada, S., Nakagomi, A., Moriya, J., Shimizu, I., Nojima, A., Yoshida, Y., Ichimiya, H., Kamimura, N., Kobayashi, Y., et al. (2014). Inhibition of endothelial p53 improves metabolic abnormalities related to dietary obesity. Cell Rep. *7*, 1691–1703.

Yoneshiro, T., Aita, S., Matsushita, M., Kayahara, T., Kameya, T., Kawai, Y., Iwanaga, T., and Saito, M. (2013). Recruited brown adipose tissue as an antiobesity agent in humans. J. Clin. Invest. *123*, 3404–3408.

STAR★METHODS

KEY RESOURCES TABLE

REAGENT or RESOURCE	SOURCE	IDENTIFIER
Antibodies		
Anti-Sirt1 Antibody	Sigma-Aldrich	Cat#07–131, RRID: AB_11214517
Pan-Actin Antibody	Cell Signaling Technology	Cat# 4968, RRID: AB_2313904
Anti-UCP1 antibody	Abcam	Cat# ab10983, RRID:AB_2241462
α-Tubulin (11H10) Rabbit mAb antibody	Cell Signaling Technology	Cat# 2125, RRID:AB_2619646
BB515 Streptavidin	BD horizon	Cat#564453: A RRID: AB_2869580
Acetyl-p53 (Lys379) Antibody	Cell Signaling Technology	Cat# 2579: RRID:AB_823591
p53 (DO-1)	Santa Cruz Biotechnology	Cat# sc-126 RRID:AB_628082
Streptavidin - Cy5	Invitrogen	Cat#434316; RRID: N/A
Cy5 Goat Anti-Rabbit IgG (H + L)	Life Technologies	Cat# A10523, RRID: AB_955056
Horseradish peroxidase-conjugated anti-rabbit immunoglobulin G	Jackson Immunoresearch	Cat#113-035-003; RRID: AB_2313567
HRP AffiniPure Goat Anti-Mouse IgG (H + L)	Jackson Immunoresearch	Cat# 115-035-003 RRID: AB_10015289
Dynabeads sheep anti-rat IgG	Invitrogen	Cat#11035; RRID: N/A
Rat anti-mouse CD45	BD Biosciences	Cat#550539; RRID: AB_2174426
Rat anti-mouse CD31	BD Biosciences	Cat# 553369; RRID: AB_394815
Bacterial and virus strains		
pENTR223.1-mSirt1 clone	DNAFORM	Cat# 100066295
Chemicals, peptides, and recombinant proteins		
Isolectin GS-IB4 From *Griffonia simplicifolia*, biotin-XX Conjugate	Invitrogen	Cat#I21414
Hoechst	Life Technologies	Cat#33258
Ex527	Sigma-Aldrich	Cat#E7034
3-(4,5-Dimethyl-2-thiazolyl)-2,5-diphenyltetrazolium Bromide	TCI	Cat#D0801
Critical commercial assays		
PrimeSTAR HS DNA Polymerase	Takara	Cat# R010A
QIAGEN/QIAquick Gel Extraction Kit	QIAGEN	Cat# 28704
Rapid DNA Dephos & Ligation Kit	Roche	Cat# 4898117001
X-tremeGENE9 DNA Transfection Reagent	Roche	Cat#06365809001
QuickTiter AAV Quantitation Kit	Cell Biolabs Inc	Cat#VPK-145
ViraBind AAV Purification Kit	Cell Biolabs Inc	Cat#VPK-140
In situ Apoptosis Detection Kit	TaKaRa	Cat#MK500
SIRT1 Activity Assay Kit (Fluorometric)	Abcam	Cat# ab156065
Experimental models: Cell lines		
HUVEC	Lonza	C2517A
Experimental models: Organisms/strains		
C57BL/6NCrSlc	SLC	RRID:MGI:5295404
Floxed *Sirt1* mice	Jackson Laboratories	RRID:IMSR_JAX:029603
UCP-1 Cre	Rosen et al., 2014	RRID:IMSR_JAX:024670
VEcadherin-BAC-CreERT2	Okabe et al., 2014	MGI:5705396

(*Continued on next page*)

Continued

REAGENT or RESOURCE	SOURCE	IDENTIFIER
Software and algorithms		
ImageJ	Schneider et al. (2012)	https://imagej.nih.gov/ij/
SPSS Statistics 24	IBM	https://www.ibm.com/products/spss-statistics
GraphPad PRISM 7.0	GraphPad Software	https://www.graphpad.com/scientific-software/prism/

RESOURCE AVAILABILITY

Lead contact

Further information and requests for resources and reagents should be directed to and will be fulfilled by the lead contact, Tohru Minamino at t.minamino@juntendo.ac.jp.

Materials availability

This study did not generate new unique reagents.

Data and code availability

All data reported in this paper will be shared by the lead contact upon request. This paper does not report original code. Any additional information required to reanalyze the data reported in this paper is available from the lead contact upon request.

EXPERIMENTAL MODEL AND SUBJECT DETAILS

Animal models

All animal experiments were conducted in compliance with the protocol, which was reviewed by the Institutional Animal Care and Use Committee of Niigata University and Juntendo University and approved by the presidents of those universities. C57BL/6NCrSlc male mice were purchased from SLC Japan (Shizuoka, Japan). Mice were housed at room temperature (24°C), with a 12 hr light–dark cycle. Some of these mice were maintained on a high fat diet (HFD; HFD32, CLEA Japan) from 4 weeks of age. Some normal chow (NC) and HFD mice were given 0.1% boysenberry polyphenols (BoyP) through their drinking water also from 4 weeks of age. HFD mice were evaluated at 12–21 weeks of age. Some NC mice were housed under thermoneutral (TN) conditions (30°C; LP-30LED-8AR, NK system) from 11 weeks of age and given the 0.1% BoyP drinking water. TN mice were evaluated at 13–15 weeks of age. *Ucp1*-Cre$^{+/-}$ mice and *Sirt1*$^{fl/fl}$ mice were crossed to generate *Ucp1*-Cre$^{+/-}$; *Sirt1*$^{fl/fl}$ (BAT-*Sirt1* KO) mice as brown adipocyte-specific *Sirt1*-KO mice. BAT-*Sirt1* KO male mice were maintained at TN condition from 13 weeks of age and evaluated at 15–24 weeks of age. Male *VE-cadherin*-BAC Cre$^{+/-}$; *Sirt1*$^{fl/fl}$ mice were crossed with female *Sirt1*$^{fl/fl}$ mice to create VE-cadherin-BAC Cre$^{+/-}$; *Sirt1*$^{fl/fl}$ mice as endothelial cell-specific *Sirt1*-KO mice (EC-*Sirt1* KO). To induce VE-cadherin-BAC Cre recombinase, EC-*Sirt1* KO male mice were administered 1 mg of tamoxifen (Sigma Life Science T5648-1G) dissolved in 200 μL of corn oil (Sigma Life Science C267-500ML) by intraperitoneal (i.p.) injection for 5 days at 11 weeks of age. Littermate control male mice (VE-cadherin-BAC Cre$^{-/-}$, *Sirt1*$^{fl/fl}$ mice) were also administrated with the same amount of tamoxifen. EC-*Sirt1* KO mice and littermate control were maintained under TN conditions from 11 weeks of age and administered 0.1% BoyP in their drinking water. EC-*Sirt1* KO mice were evaluated at 13–23 weeks of age. Mice were euthanized by i.p barbiturate injection, then tissues were collected.

METHOD DETAILS

Boysenberry polyphenols

Boysenberry juice was obtained from Berryfruit Export New Zealand Ltd. (New Zealand). Boysenberry polyphenols (BoyP) were prepared as previously reported (Furuuchi et al., 2018). In short, BoyP were purified from boysenberry juice with an Amberlite XAD-7HP column (Organo, Japan) and loaded to a Dowex 50W-X8 column (Dow Chemical, US). The column was washed with ethanol, water, and formic acid in a ratio of 80:20:1, and the anthocyanin fraction (BoyAC) was eluted with ethanol, water, and hydrochloric acid in a ratio of 50:50:10. Concentration for BoyAC in boysenberry juice were 101 mg/dl in year 2009, 80 mg/dl in year 2010, 71 mg/dl in year 2016.

Isolation of ECs

BAT was harvested from mice, and ECs were isolated as previously reported (Yokoyama et al., 2014). In short, tissues were digested by 1.2 units mL^{-1} of Dispase II (EIDIA, Japan), 2 mg mL^{-1} type IV collagenase (Worthington, NJ), and 2mM CaCl2 in phosphate-buffered saline (PBS) for 30 min at 37°C. The tissue digestion factors were neutralized by Dulbecco's Modified Eagle Medium containing 10% fetal bovine serum (FBS) and passed through 70-μm and 40-μm filters. Then, the samples were centrifuged at 300*g* for 5 min and re-suspended in magnetic-activated cell sorting (MACS) buffer (PBS with 1% FBS and 2mM EDTA). The MACS technique was used to remove $CD45^+$ cells from the cells and collect $CD31^+$ cells. MACS was performed with anti-CD45 microbeads and anti-CD31 microbeads (Miltenyi Biotec, Germany).

Glucose tolerance test

The glucose tolerance test (GTT) was performed as previously reported (Shimizu et al., 2014). On the day of the GTT, mice were fasted for 6 h, and glucose was administered intraperitoneally (i.p.) at a dose of 1 g/kg body weight. At 0, 15, 30, 60, and 120 min after i.p. injection, blood glucose levels in tail blood were measured by a glucose analyzer (SANWA KAGAKU KENKYUSHO).

Cold tolerance test

The cold tolerance test (CTT) was performed as previously reported (Shimizu et al., 2014). Body temperature was measured by subcutaneously implanting microchip transponders (IPTT-300 Extended Accuracy Calibration; Bio Medic Data Systems) in the scapular region according to the manufacturer's instructions. For the acute CTT, mice were placed in a room at 4°C, and body temperature was measured every hour for up to 8 h. (In the long CTT, at 9 am mice were placed in a room at 4°C, and their body temperature was measured at 9 am every day.) In both the acute and long CTTs, the mice were judged to have severe hypothermia when their body temperature was below 33°C, at which point they were moved to room temperature.

Plasma insulin level

After 6 h' fasting, blood was collected from the tail vein and heparinized to obtain plasma. Then, plasma insulin levels were measured according to the instructions of the measurement kit (Morinaga Institute of Biological Science Inc., M1104).

Histological analysis

BAT was harvested, fixed overnight in 10% formalin, embedded in paraffin and sectioned for hematoxylin and eosin (HE) or immunofluorescence staining. The number of large lipid droplets (defined as droplets with a surface area >250 μm^2) in the ×400 field was counted. For immunofluorescence, the sections were deparaffinized and retrieved with 10mM citrate buffer (pH 6.0). As the first antibody, anti-SIRT1 (Sigma-Aldrich, 07–131) was used, together with isolectin GS-IB4 (IB4, derived from *Griffonia simplicifolia*-biotin-XX conjugate) for staining of capillaries (Invitrogen, I21414), and Hoechst (Life Technologies, 33258). Secondary antibodies were Cy5 Goat anti-rabbit IgG (H + L; Life Technologies, A10523) for anti-Sirt1, BB515 streptavidin (BD horizon, 564453), and Cy5-streptavidin conjugate (Invitrogen, 43–4316) for IB4. TUNEL staining was performed to assess apoptosis. The sections were stained according to the instructions of the *In situ* Apoptosis Detection Kit (TaKaRa, MK500). HE-stained images were captured with a Biorevo microscope system (Keyence Co.), and immunofluorescence sections were assessed by confocal microscopy (NIKON, C2). ImageJ was used to quantify image analysis (Schneider et al., 2012).

RNA analysis

Total RNA was isolated from tissue samples with RNAbee (TEL-TEST Inc.). Quantitative polymerase chain reaction (qPCR) was performed by using a Light Cycler 480 (Roche) with the Universal Probe Library and the Light Cycler 480 Probes Master (Roche) according to the manufacturer's instructions.

The primers and their sequences were as follows:

Ucp1: 5'-ggcctctacgactcagtcca-3', 5'-taagccggctgagatcttgt-3'.

Ppargc1a: 5′- gaaagggccaaacagagaga-3′, 5′- gtaaatcacacggcgctctt-3′.

28S: 5′-atatccgcagcaggtctcc-3′, 5′-gccgacttcccttacctaca-3′.

Respiratory gas analysis

Oxygen consumption was measured in mice with the O2/CO2 metabolism measurement system (Columbus Instruments) according to the manufacturer's instructions.

Western blot analysis

Protein lysate was extracted with RIPA (10mM Tris-HCl, pH 8, 140mM NaCl, 5mM EDTA, 0.025% NaN3, 1% Triton X-100, 1% deoxycholate, 0.1% sodium dodecyl sulfate [SDS]) with a protease inhibitor cocktail (Roche, 11873580001). The lysates were separated by SDS polyacrylamide gel electrophoresis, and the proteins were transferred to a polyvinylidene difluoride membrane. Anti-Sirt1 (Sigma-Aldrich, 07–131), anti-α-tubulin (Cell signaling technology, 2125), Acetyl-p53 (Lys379) Antibody (Cell Signaling Technology, 2579), p53 (DO-1) (Santa Cruz Biotechnology, sc-126) and Ucp1 (Abcam, ab10983) were used as primary antibodies at a concentration of 1:1000, and 5% skim milk was used for blocking. Horseradish peroxidase-conjugated anti-rabbit immunoglobulin-G (Jackson, 115-035-144) and HRP AffiniPure Goat Anti-Mouse IgG (H + L) (Jackson, 115-035-003) were used as the secondary antibody at a concentration of 1:5000. The proteins were detected by enhanced chemiluminescent Western blotting detection reagents (GE Healthcare). As a positive control for acetyl-p53, 400 nM trichostatin A and 0.5 μM doxorubicin were reacted with HUVECs for 24 h.

Cell culture and viability test

Human umbilical vein endothelial cells (HUVECs, Lonza) were cultured with an Endothelial Cell Growth Medium-2 BulletKit (EGM-2, Lonza). Cell viability was evaluated by 3-(4,5-dimethyl-2-thiazolyl)-2,5-diphenyl-2H-tetrazolium bromide (MTT) assay (Plumb, 1999), and 1 μg/mL BoyP or BoyAC, 100 μM palmitic acid (PA), and 10 μM EX 527 were added to the cells as Sirt1 inhibitors. Then, 24 h after the addition of the reagent, the medium was removed, and 0.5 mg/mL MTT in endothelial growth medium 2 was added. After 3.5 h, the MTT solution was removed and dissolved in dimethyl sulfoxide. The solution was measured at 540 nm by a microplate reader (Bio-Rad, iMark).

Adeno-associated virus

The purified adeno-associated virus mSirt1 (pAAV-mSirt1) vector was constructed with a pENTR223.1-mSirt1 clone (DNAFORM). The mSirt1 target site was obtained from pENTR223.1-mSirt1 with PrimeSTAR HS DNA Polymerase by using GC Buffer and primers, with ClaI and BglII as linkers. The mSirt1 obtained by electrophoresis was purified with a QIAGEN/QIAquick Gel Extraction Kit. The mSirt1 was ligated into the pAAV with the Rapid DNA Dephos & Ligation Kit, transformed into *E. coli* JM109 Competent Cells and then selected by ampicillin. The pAAV-mSirt1 was purified with an OriGnene MaxiPrep kit. Then, pAAV-mSirt1 vector and pAAV-GFP vector were co-transfected into HEK293 cells with pAAV-DJ and pHelper by using a transfection reagent (X-tremeGENE9 DNA Transfection Reagent, Roche, 06365809001). The AAV was extracted by freeze-thawing and purified with ViraBind AAV Purification Kit (Cell Biolabs Inc, VPK-140). The titer of AAV was quantified with QuickTiter AAV Quantitation Kit (Cell Biolabs Inc, VPK-145). AAV was directly injected by visualization at a concentration of 1 × 10^9 GC/mice into BAT of HFD male mice (17 weeks of age). Physiological studies were started 14 days after infection.

SIRT-1 activity analysis

SIRT-1 activity was analyzed with SIRT1 Activity Assay Kit (abcam, ab156065) according to the manufacturer's instructions. Recombinant SIRT-1 was preincubated with or without 1 μg/mL BoyP for 10 min and then reacted with fluoro-substrate peptide for 10 min. The fluorescence intensity produced by the deacetylation of the substrate was measured by NIVO using an excitation wavelengths of 350 nm and emission wavelengths of 460 nm.

QUANTIFICATION AND STATISTICAL ANALYSIS

Statistical analysis

Statistical analyses were performed with SPSS software, version 24. Graphs were plotted using SPSS and GraphPad PRISM 7.0. Outliers were defined as those greater than 1.5 times the interquartile range of

the boxplots and were detected by SPSS and removed from the graphs and analyses. The exclusion of outlier is described in the figure legends. All data are from different biological replicates. Differences between groups were examined by the two-tailed Student's *t* test or one-way analysis of variance (ANOVA), followed by Tukey's multiple comparison test or by Dunnett's test for comparisons of three or more groups. Survival curves were calculated by the Kaplan-Meier method and were compared with the log-rank test. Data from some experiments were analyzed by repeated measures ANOVA followed by Tukey's multiple comparison test. In all analyses, a p value of less than 0.05 was considered statistically significant.